

ORIGINAL PAPER

A mathematical algorithm of the facial symmetry plane: Application to mandibular deformity 3D facial data

Yujia Zhu^{1,2,3,4,5,6}  | Xiangling Fu^{7,8} | Lei Zhang^{1,2,3,4,5,6} | Shengwen Zheng^{7,8} |
Aonan Wen^{1,2,3,4,5,6} | Ning Xiao^{1,2,3,4,5,6} | Yong Wang^{1,2,3,4,5,6} | Yijiao Zhao^{1,2,3,4,5,6}

¹Center of Digital Dentistry/Department of Prosthodontics, Peking University School and Hospital of Stomatology, Beijing, PR China

²National Center of Stomatology, Beijing, PR China

³National Clinical Research Center for Oral Diseases, Beijing, PR China

⁴National Engineering Laboratory for Digital and Material Technology of Stomatology, Beijing, PR China

⁵Beijing Key Laboratory of Digital Stomatology, Beijing, PR China

⁶Research Center of Engineering and Technology for Computerized Dentistry Ministry of Health, Beijing, PR China

⁷School of Computer Science, Beijing University of Posts and Telecommunications (National Pilot Software Engineering School), Beijing, PR China

⁸Key Laboratory of Trustworthy Distributed Computing and Service, Ministry of Education, Beijing University of Posts and Telecommunications, Beijing, PR China

Correspondence

Yong Wang and Yijiao Zhao, No.22 Zhongguancun South Avenue, Haidian District, Beijing, 100081, PR China.
Emails: kqcadc@bjmu.edu.cn; kqcadcs@bjmu.edu.cn

Funding information

Key R&D Program of Ningxia Hui Autonomous Region of China, Grant/Award Number: 2018BEG02012; Open Subject Foundation of Peking University Hospital of Stomatology, Grant/Award Number: PKUSS20190501; National Natural Science Foundation of China, Grant/Award Number: 81870815 and 82071171

Abstract

The three-dimensional (3D) symmetry reference plane (SRP) is the premise and basis of 3D facial symmetry analysis. Currently, most methods for extracting the SRP are based on anatomical landmarks measured manually using a digital 3D facial model. However, as different clinicians have varying definitions of landmarks, establishing common methods suitable for different types of facial asymmetry remains challenging. The present study aimed to investigate and evaluate a novel mathematical algorithm based on power function weighted Procrustes analysis (PWPA) to determine 3D facial SRPs for patients with mandibular deviation. From 30 patients with mandibular deviation, 3D facial SRPs were determined using both our PWPA algorithms (two functions) and the traditional PA algorithm (experimental groups). A reference plane, defined by experts, was considered the 'truth plane'. The 'position error' index of mirrored landmarks was created to quantitatively evaluate the difference among the PWPA SRPs and the truth plane, including overall differences and regional differences of the face (upper, middle and lower). The 'angle error' values between the SRPs and the truth plane in the experimental groups were also evaluated in this study. Statistics and measurement analyses were used to comprehensively evaluate the clinical suitability of the PWPA algorithms to construct the SRP. The average angle error values between the PWPA SRPs of the two functions and the truth plane were $1.21 \pm 0.65^\circ$ and $1.18 \pm 0.62^\circ$, which were smaller than those between the PA SRP and the truth plane. The position error values of mirrored landmarks constructed using the PWPA algorithms for the whole face and for each facial partition were lower than those constructed using the PA algorithm. In conclusion, for patients with mandibular deviation, this novel mathematical algorithm provided a more suitable SRP for their 3D facial model, which achieved a result approaching the true effect of experts.

KEYWORDS

aesthetics, facial asymmetry, oral diagnosis, orthodontics, orthognathic surgical procedures, three-dimensional imaging

1 | INTRODUCTION

Facial symmetry and coordination are important factors in facial and oral aesthetics and have a marked influence on the attractiveness of individuals (Grammer & Thornhill, 1994; Hönn & Göz, 2007; Hönn et al., 2005; Mealey et al., 1999; Zaidel et al., 2005). However, no human face is perfectly symmetrical (Berssenbruegge et al., 2015; Shaner et al., 2000; Zaidel & Cohen, 2005). Therefore, the symmetry analysis of a three-dimensional (3D) face is an important part of the orthodontic design, oral and maxillofacial surgery planning, assessment of the impact of facial growth on facial appearance and prosthodontic aesthetic design (Al Rudainy et al., 2019a, 2019b; Haraguchi et al., 2008; Lee et al., 2010; O'Grady & Antonyshyn, 1999; Philipp et al., 2011; Verhoeven et al., 2016).

The 3D symmetry reference plane (SRP) (also referred to as the median sagittal plane) is the premise and foundation of 3D facial symmetry analysis and reconstructive procedures. Landmark-based methods have been widely used in previous studies to determine the SRP (Djordjevic et al., 2014; Huang et al., 2013; Hyeon-Shik et al., 2012; Plooj et al., 2009). Lee et al. (2014) proposed the plane perpendicular to the horizontal reference plane and passing through the right and left endocanthions as the midsagittal reference plane to analyse the facial symmetry of orthodontic patients with mandibular deviation. Murakami et al. (2014) fitted the median sagittal plane from six midline facial landmarks—the nasion, pronasale, subnasale, labiale superius, labiale inferius and pogonion of soft tissue—and compared the facial symmetry between normal male Japanese adults and children. Thus, the reference landmarks for different researchers are not exactly the same (Masoud et al., 2016).

Recently, the SRP-determined method developed by Hartmann et al. (2007) has gradually attracted attention; it can be determined by superimposing the original and its mirror facial image. The central notion of this method is to obtain the 3D optimal overlap between the original and the mirror model, mainly consisting of the iterative closest point (ICP) and Procrustes analysis (PA) algorithms (Besl & McKay, 1992; Damstra et al., 2011; Du et al., 2017). The ICP algorithm is an iterative method that seeks the local minimum solution, with its objective function defined by the Euclidean distance between the nearest points. It involves a high degree of automation and repeatability and does not refer to the facial anatomical landmarks information (Chen & Medioni, 1992; Stewart et al., 2003). However, it is unsuitable for complex facial deformities because of the influence of deformed regions. At present, such cases require manual screening of non-deformed facial region data to ensure the accuracy of the SRP ('regional ICP algorithm' or 'expert ICP') (De Momi et al., 2006; Verhoeven, Nolte, et al., 2013). Verhoeven, Coppen, et al. (2013) selected regions consisting of the forehead, upper nasal dorsum and zygoma which were found to have the least temporal variability and to be the most suitable to register two 3D photographs of the same person.

The PA algorithm focuses on facial landmarks, anatomical landmarks or a mathematical facial mask, which are more aligned with clinical experience and diagnostic practices. It obtains the optimal overlapping position with the minimum average distance between

the original and the corresponding mirror landmarks through a matrix operation (translating, rotating and scaling). The least-square superimposition method was adopted to find the optimal position. Damstra et al. (2011) applied the PA algorithm to construct a 3D craniofacial SRP of cone beam computed tomography skull data and confirmed its reliability. Facial asymmetry assessment based on a mathematical facial mask consists of several indexed vertices that fully describe the complexity of facial morphology, which may allow a comprehensive analysis of facial asymmetry. Meanwhile, it can simplify the operation process and increase repeatability (Ailrudainy et al., 2018; Claes, Walters, Shriver, et al., 2012). Xiong et al. (2016) used the PA algorithm to compute the midsagittal plane for subjects with no apparent facial asymmetry based on 21 anatomical landmarks. However, for patients with noticeable facial asymmetry, this method is not ideal because the algorithm assigns equal weight to individualised facial features without discrimination, which deviates from the rationale followed in clinical diagnosis. Zhu et al. (2020) proposed the weighted Procrustes analysis (WPA) algorithm which provides a more adaptable SRP than the standard PA algorithm when applied to mandibular deviation patients.

This study was conducted to obtain a more accurate facial SRP construction. To this end, we optimised the weight functions of facial anatomical landmarks based on previous research to better simulate the diagnosis strategies of clinical experts. Two power function expressions of anatomical landmarks 'segmented power function weighted Procrustes analysis (SPWPA)' and 'offset PWPA (OPWPA)' were applied in this study for patients with mandibular deviation. The results showed similar effects to those of clinical experts.

2 | METHODS

2.1 | Subjects

Thirty participants from Peking University School and Hospital of Stomatology aged between 18 and 35 years were enrolled. The inclusion criteria were apparent facial asymmetry with a mandibular deviation of at least 3 mm from the facial midline, which is perpendicular to the interpupillary line at the soft tissue nasion when the patient is seated in a natural head position. All procedures were safe, non-invasive and did not provoke pain or discomfort in the subjects. This study was approved by the Ethics Committee of Peking University School and Hospital of Stomatology (PKUSSIRB-202054042), and written informed consent was obtained from all participants.

2.2 | Experimental equipment and software

A Face Scan 3D sensor system (3D-Shape Corp.) was used to collect 3D facial data for each patient. We obtained facial data in only 0.8 s with high accuracy of 0.1 mm and a scanning range of 270–320°.

For data processing, we used the reverse engineering software Geomagic Studio 2013 (3D Systems Inc), which processes 3D facial data and extracts the SRP. The PWPA algorithm optimises the objective function based on the PA algorithm by assigning weights to landmarks, using a weighted least-squares superimposition; this was implemented in Python (the algorithms are open source and available at <https://github.com/cadcgrou/WPA>). The PWPA objective function F' is shown in Equation (1). According to the weight function (W_i) in Equation (1), this study constructed two functions: segmented power (SP) function and offset power (OP) function, the weight function of which is shown in Equations (2 and 3). The function graph is shown in Figure 1.

$$F' = \min_Q \sum_{i=1}^p W_i \| \text{LMK_Org}_i - \text{QLMK_Mir}_i \|_2, \quad (1)$$

$$W = \begin{cases} 1, & 0 \leq D \leq 1 \text{ mm} \\ \frac{1}{D}, & D > 1 \text{ mm} \end{cases}, \quad (2)$$

$$W = \frac{1}{D+1} (D \geq 0), \quad (3)$$

where LMK_Org represents the original model landmark set, LMK_Mir represents the mirror model landmark set, LMK_Org_{*i*} and LMK_Mir_{*i*} ($i = 1, 2, \dots, 32$) are the corresponding landmarks in the original and mirror landmark sets, Q is the spatial change matrix (contains translation, rotation and scale; the value of the scale is one in this study) and p is the number of landmarks. The value of W in this study is W_p , W_i ($i = 1, 2, \dots, 32$) is the weight factor for each facial landmark, and D is the distance between the original and corresponding mirror landmarks.

2.3 | Facial model acquisition and processing

The equipment was calibrated before capturing 3D facial data, and each patient was guided by the clinician to a natural head position. Geomagic Studio 2013 software was used for image processing. We first adjusted the Frankfort horizontal plane of the original 3D model to coincide with the XZ plane of the global coordinate system. One experienced senior

clinical professor created anatomical landmarks from each original facial model (Model_Org). Then, 32 original anatomical landmarks were selected from the whole face, including the nasion, pogonion, endocanthion and alare landmarks, as shown in Figure 2. The process to calculate the mean coordinate of LMK_Org was repeated three times by a senior clinical professor with years of experience in digital surgery or prosthodontics and the data were saved in OBJ file format.

2.4 | Abstracting the SRP

Initial alignment of Model_Org and its YZ-plane mirror model was performed, based on the global ICP registration function in Geomagic Studio 2013 software. After alignment, the mirror model (Model_Mir) and the corresponding initial LMK_Mir were established.

2.4.1 | Experimental group_1: Extracting the SRP with the PA algorithm

The 3D coordinates of all 32 pairs of landmarks were imported into the PA algorithm program in Python. The transformation matrix (translation and rotation) of the mirror model was then calculated based on the least-squares method and the matrix was loaded onto Model_Mir using Geomagic Studio 2013 software in the .tfm format. Based on the composition of the original and mirror models, the SRP of the original model was constructed (SRP_PA) using the 'symmetry' function in Geomagic Studio 2013.

2.4.2 | Experimental group_2 and Experimental group_3: Extracting the SRPs with the PWPA algorithms

LMK_Org and LMK_Mir were inputted into a Python program that runs the SPWPA and OPWPA algorithms. In this process, the weight of each landmark was calculated automatically based on the SP and OP functions (Figure 1). In this study, the SP and OP functions were used to

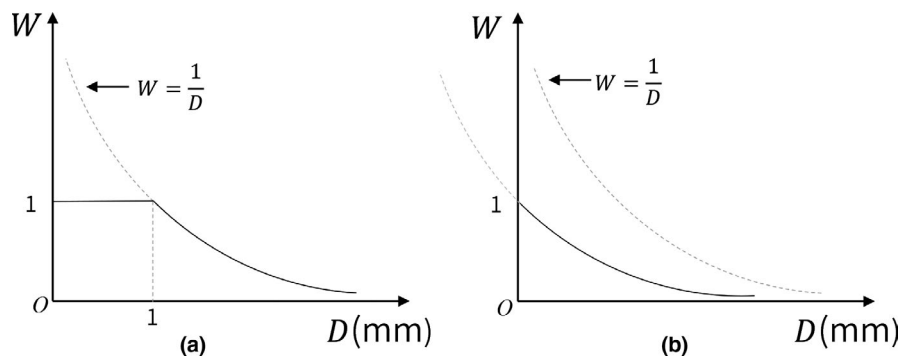


FIGURE 1 Function graphs of segmented power and offset power. (a) Segmented power function. (b) Offset power function. D is the distance between the original and mirror corresponding landmarks. W is the weight factor for each facial landmark. The dashed function image is the original power function $W = 1/D$

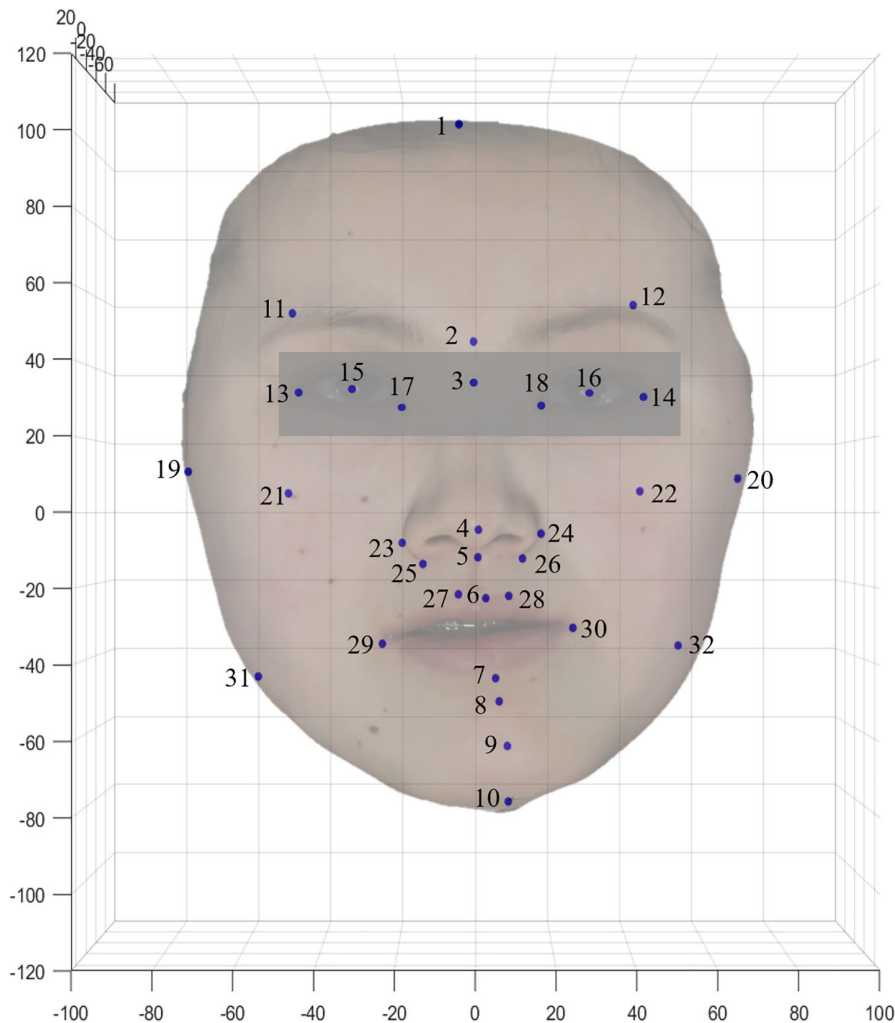


FIGURE 2 The 32 anatomic landmarks (Upper facial third: 1-trichion, 2-glabella, 11–12-superciliary ridge; Middle facial third: 3-nasion, 4-pronasale, 5-subnasale, 13–14-exocanthion, 15–16-pupil, 17–18-endocanthion, 19–20-tragion, 21–22-zygion, 23–24-alare, 25–26-subalare; Lower facial third: 6-labiale superius, 7-labiale inferius, 8-sublabiale, 9-pogonion, 10-gnathion, 27–28-crista philtre, 29–30-cheilion, 31–32-gonion)

achieve the effect of a landmark pair with good symmetry that would be relatively close together after initial registration and, thus, would be given more weight. The weights of all the anatomical landmarks were distributed in a reasonable domain which was more appropriate than the previous WPA algorithm (Zhu et al., 2020). The weighted landmarks of LMK_Org and LMK_Mir were superimposed three-dimensionally based on the least-squares method; thus, optimal overlapping was obtained for the 32 pairs of landmarks, and the SPWPA and OPWPA transformation matrices of Model_Mir were obtained. The transformation matrices were loaded into Model_Mir using Geomagic Studio 2013 software separately in .tfm format. The SRP of the facial data for each of the 30 patients was constructed as described (SRP_SPWPA and SRP_OPWPA).

2.4.3 | Reference group: Abstracting the truth plane

De Momi et al. (2006) showed that the symmetry plane based on the regional ICP algorithm is reliable and leads to no significant difference

from that constructed by experienced clinicians. In this study, the facial SRP constructed by this 'regional ICP algorithm' was regarded as the truth plane. Three senior professors with considerable experience in digital surgery and skilled in operating computer software selected regions of good facial symmetry from Model_Org and Model_Mir using Geomagic Studio 2013 software, and 'regional registration' was carried out with the two models. Finally, the average SRP of the facial data was extracted as the ground truth (SRP_Tru).

The SRPs extracted using the SPWPA, OPWPA, PA algorithms and truth plane are depicted in Figure 3.

2.5 | Measurement evaluation of SRP

2.5.1 | Angle error of planes

For each of the 30 3D models, the angles between the SRPs of the experimental groups and the truth plane were calculated and

recorded as Ang_SPWPA, Ang_OPWPA and Ang_PA. The mean and standard deviation of the angle error were calculated for all groups.



FIGURE 3 Determining the SRP based on the PWPA algorithms, PA algorithm and regional iterative closest point algorithm for one case. The red plane signifies the SRP of ground truth, the blue plane represents the segmented PWPA algorithm, the green plane represents the offset PWPA algorithm and the yellow plane represents the PA algorithm. PA, Procrustes analysis; PWPA, power function weighted Procrustes analysis; SRP, symmetry reference plane

2.6 | Position error of the mirrored landmarks

The position error of the mirrored landmarks was a new quantitative index to assess the SRP to validate the effect of the weighted landmarks. The mirror landmarks of the experimental groups (Mir_SPWPA, Mir_OPWPA and Mir_PA) were obtained from the mirror and original models using SRP_SPWPA, SRP_OPWPA and SRP_PA, and the mirror landmarks of the truth group were similarly obtained (Mir_True). The overall position error was defined as the average distance of the 32 pairs of landmarks in the experimental groups and the truth group, named LMK_SPWPA, LMK_OPWPA and LMK_PA (Figure 4). The regional position error of three facial parts was also tested in the study, which was calculated for landmarks in the upper third (4 landmarks), middle third (17 landmarks) and lower third (11 landmarks) facial regions, termed as LMK_SPWPA_Up, LMK_OPWPA_Up and LMK_PA_Up; LMK_SPWPA_Mid, LMK_OPWPA_Mid and LMK_PA_Mid and LMK_SPWPA_Low, LMK_OPWPA_Low, and LMK_PA_Low, respectively. The mean and standard deviation of the overall and regional position errors were calculated for each sample.

2.7 | Statistical analysis

Statistical analyses were carried out using SPSS software, Version 21. To investigate the intra-observer error, the senior clinical professor repeated the landmark measurements for nine facial models 1 week later, and the intra-class coefficient (ICC) was calculated.

A Kolmogorov–Smirnov normality test was conducted for angle error and position errors to examine the distribution of the data. A parametric or non-parametric test was then used depending on the results. The workflow of the experimental procedures and evaluation methods is shown in Figure 5. Statistical analysis of the angle error of the SPWPA, OPWPA and PA algorithms was performed

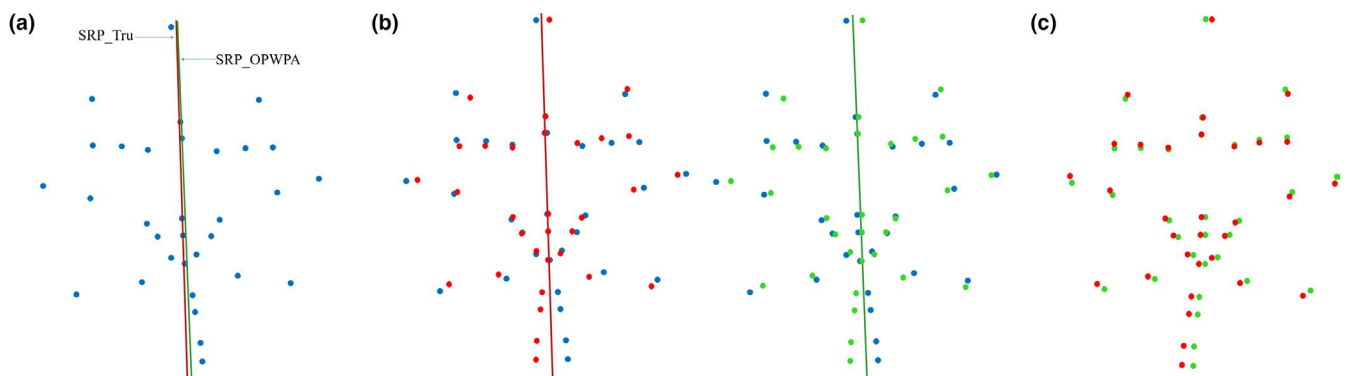


FIGURE 4 Position error of the mirrored landmarks. (a) SRPs on the original facial landmarks (blue); the red plane signifies the ground truth (SRP_True) and the green represents the PWPA algorithm plane (SRP_OPWPA). (b) Reference mirror landmarks in red and OPWPA mirror landmarks in green, which were obtained from the mirror original landmarks using SRP_True and SRP_OPWPA. (c) Global position error was defined as the average distance of the 32 pairs of reference and OPWPA mirror landmarks. OPWPA, offset PWPA; PWPA, power function weighted Procrustes analysis; SRP, symmetry reference plane

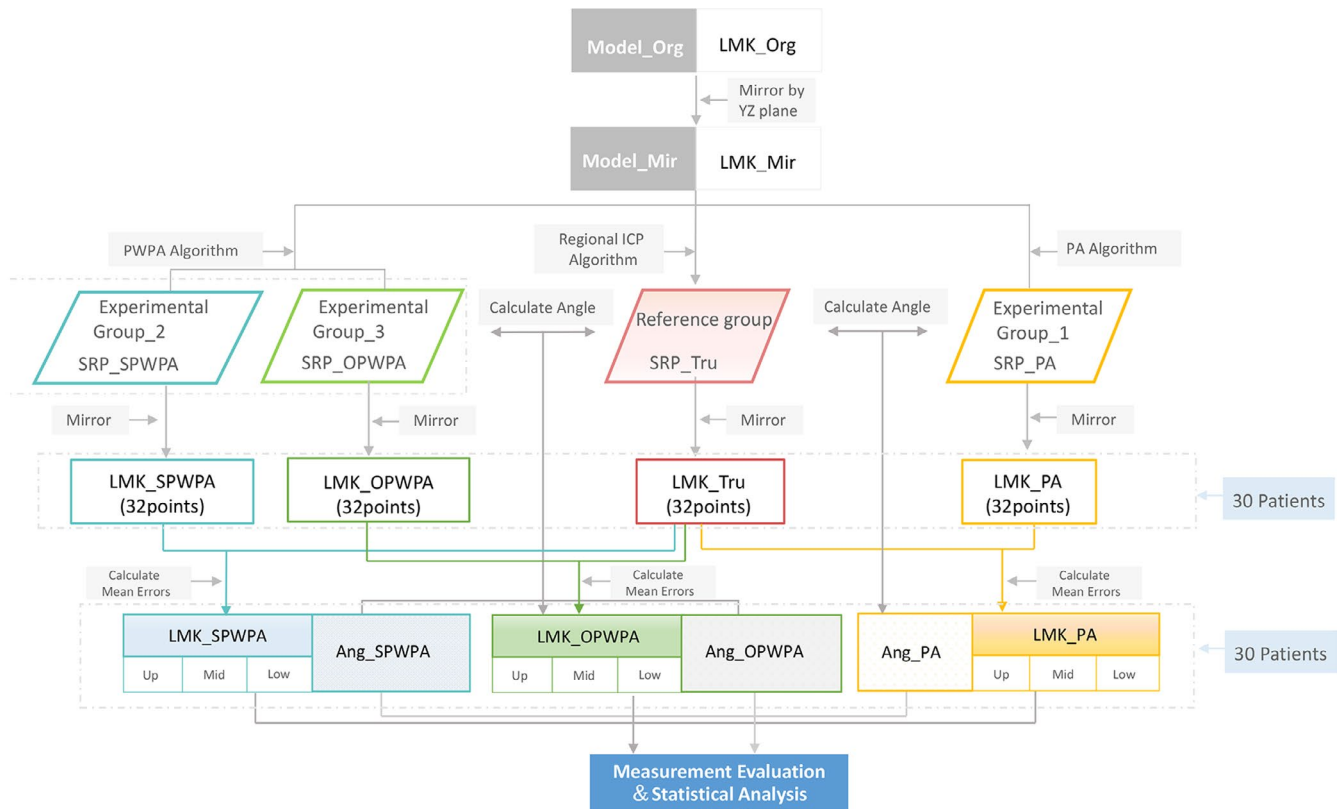


FIGURE 5 Workflow of the experimental procedures and evaluation methods. PWWA represents the power function weighted Procrustes analysis (PA) algorithm, and PA represents the PA algorithm. SRP_SPWPA, SRP_OPWPA, SRP_PA and SRP_True are symmetry reference planes constructed based on the experimental group and the truth group. Mir_SPWPA, Mir_OPWPA, LMK_PA and Mir_True are mirror landmarks constructed with the PWWA algorithms, PA algorithm SRP and truth plane. LMK_SPWPA, LMK_OPWPA and LMK_PA are the overall landmark position errors of the PWWA and PA algorithms under which Up, Mid and Low represent the position errors of different third parts. Ang_SPWPA, Ang_OPWPA and Ang_PA are the angle errors of the PWWA algorithm and PA algorithm groups. OPWPA, offset PWWA; PWWA, power function weighted Procrustes analysis; SPWPA, segmented PWWA; SRP, symmetry reference plane

using one-way analysis of variance (ANOVA). Homogeneity of variance test and Tukey's multiple comparison test were also performed.

One-way ANOVA and Tukey's multiple comparison test were subsequently performed for the overall and regional position errors. The statistical significance was set at $p < 0.05$. One-way ANOVA was performed for regional landmarks of the position error to examine whether differences in the position error of different facial parts were statistically significant.

3 | RESULTS

For all analysed measures of landmark detection by one expert, the intra-observer ICC values were >0.95 (0.97–0.99), demonstrating high intra-observer reproducibility.

3.1 | Analysis of angle error

The angle errors of the SRPs of the 30 samples (using the PA, SPWPA and OPWPA algorithms) of mandibular deviation were calculated.

The Kolmogorov–Smirnov normality test for angle error (three groups with 30 values each) showed that all groups conformed to the normal distribution. Data analysis yielded statistically significant differences ($p < 0.05$) between the experimental groups; Tukey's multiple comparison test showed that the difference in the angle error between the PA, SPWPA and OPWPA algorithms was statistically significant. The mean and standard deviation of the angle error in the PA, SPWPA and OPWPA groups were $2.12 \pm 0.81^\circ$, $1.18 \pm 0.62^\circ$ and $1.21 \pm 0.65^\circ$, respectively, indicating that the SRP extracted using the PWWA algorithm was closer to the truth group for the 30 samples.

The degree of mandibular deviation for each patient was calculated using the distance from the pogonion to the truth plane as defined by the experts, and the angle error distribution of 30 patients with different degrees of deviation was analysed as shown in Figure 6. The results suggested that the angle error of each algorithm increased with the increase in the degree of mandibular deviation. However, for patients with noticeable mandibular deviation, the PWWA algorithm was optimised compared with the PA algorithm without weight allocation, and there was no significant difference between the SPWPA algorithm and the OPWPA algorithm.

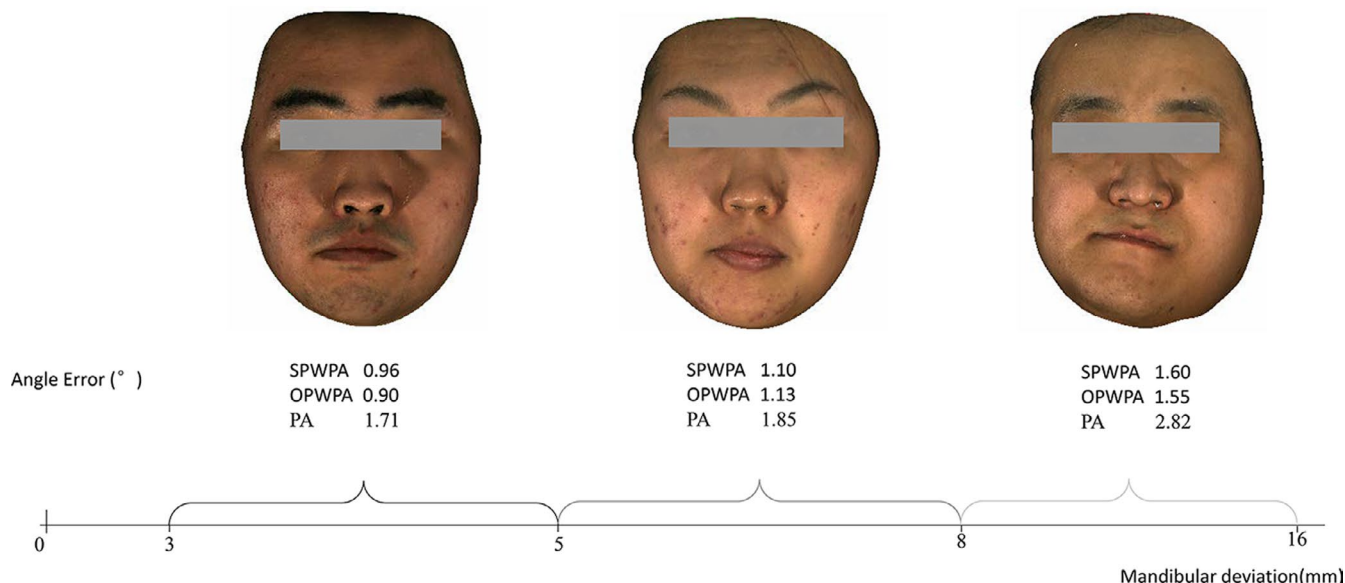


FIGURE 6 Angle error of different degrees of mandibular deviation patients

TABLE 1 Position error of overall and regional facial landmarks (upper, middle and lower) (mm)

Position error (mm)	PA	SPWPA	OPWPA
LMK	4.08 ± 0.65	2.99 ± 1.33	2.98 ± 1.33
LMK_Up	3.57 ± 1.67	1.89 ± 0.98	1.90 ± 1.00
LMK_Mid	3.41 ± 1.22	2.64 ± 1.18	2.62 ± 1.14
LMK_Low	5.29 ± 2.67	3.90 ± 1.92	3.91 ± 1.97

Abbreviations: LMK_Low, lower landmark; LMK_Mid, middle landmark; LMK_Up, upper landmark; OPWPA, offset power function weighted Procrustes analysis; SPWPA, segmented power function weighted Procrustes analysis.

Taken together, a more ideal SRP can be obtained with the PWPA algorithm.

3.2 | Analysis of position error

The measurement values for the position error of the experimental groups for overall landmarks (three groups) and regional landmarks (nine groups) are presented in Table 1. All groups conformed to the normal distribution. There were significant differences in the overall position errors among the groups and regional position errors of the upper, middle and lower facial partitions ($p < 0.05$) (Figure 7).

Tukey's test showed statistically significant differences ($p < 0.05$) between the PA and SPWPA groups in the overall position error, between the PA and OPWPA groups in terms of overall position error, between the lower and upper facial partitions and between the lower and middle partitions in the PWPA and PA groups.

The overall position error and regional position errors of the PWPA groups were smaller than those of the PA group (Table 1).

The weighted overlap of the lower partition showed that the SPWPA and OPWPA groups were closer to the weighted overlap result of the truth group, revealing a significant improvement in the PWPA groups compared with the PA group.

4 | DISCUSSION

A central problem in the original-mirror alignment method is the superimposition algorithm. This study has proposed a way to improve the standard PA algorithm by adding a weighted system.

Previous studies reported alternatives such as deleting the obvious asymmetric landmarks (outliers) and using the remaining landmarks for the PA operation to avoid interference (Gateno et al., 2015; Linde & Houle, 2009; Xiong et al., 2016). Torcida et al. improved the superimposition based on resistant-fit methods by using median-based parameter estimates that are less affected by the presence of larger differences in the relative locations of a few landmarks (Sebasti et al., 2016). In this way, we proposed a weighted strategy to improve the universality of the algorithm, the mathematical model of the PWPA algorithm is an innovation based on the original mirror alignment method. The weighting strategy of the anatomical landmarks is the core of the algorithm.

In oral clinical practice, physicians tend to focus more on the landmarks with good facial symmetry (i.e., landmarks around the eyes, nose and mouth). Therefore, the power function $y = x^\alpha$ ($\alpha = -1$) was used in our previous study to demonstrate the trend in which the weight decreases with the increase of asymmetry (Zhu et al., 2020). After the initialisation of the original method and the mirror model overlaps, the landmarks with poor symmetry (in which the distance of the original mirror paired landmarks is larger) are assigned smaller weights. However, our previous study found that the power function presents a large upward trend of weights (close to infinity)

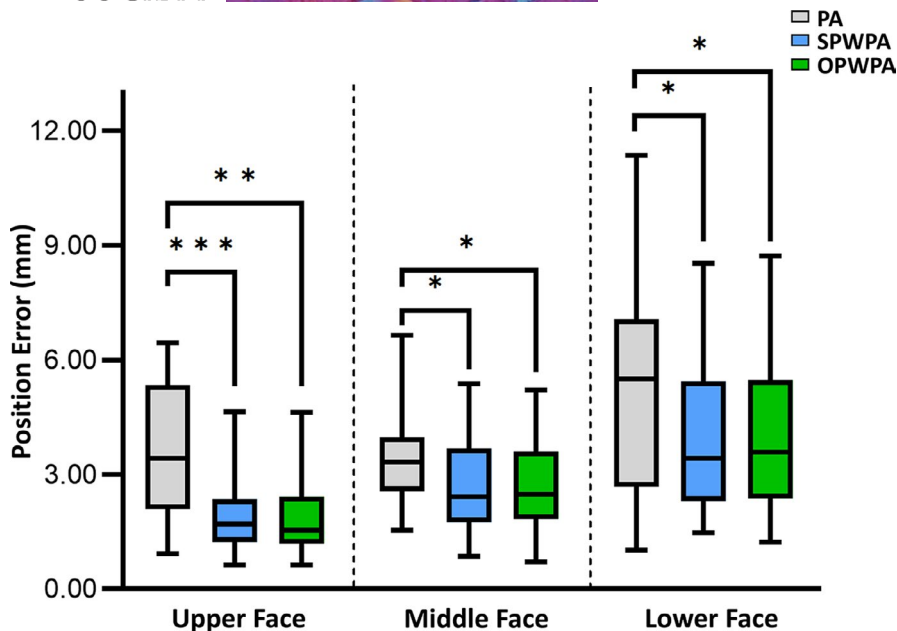


FIGURE 7 Boxplot of position error for the upper face, middle face and lower face groups. The asterisks signify $p < 0.05$ between the PWPA algorithm and PA algorithm groups. OPWPA, offset PWPA; PA, Procrustes analysis; PWPA, power function weighted Procrustes analysis; SPWPA, segmented PWPA

in the interval, where D is close to zero. It gives too much weight to some landmarks, which leads to a great difference between the high and low weights, overlapping problems may appear in some cases.

By analysing the power function expression, the absolute value of the derivative of the function was found to be larger in the interval, where D is <1 but smaller in the interval, where D is >1 ; thus, one is the critical value of the function. Therefore, based on the function characteristics (D) in this study, the power functions were improved in two forms, namely, the SP and OP functions, which reduce the distribution range of W_i and make different features contribute appropriately in the process of overlapping.

Firstly, the SP function treats the landmarks with good symmetry ($D \leq 1$ mm) equally ($W_i = 1$), because it is difficult to distinguish the importance of some anatomical landmarks in clinical application. It generally sets $D = 1$ mm as the boundary and uniformly assigns the weight of $D < 1$ mm as the upper limit of the weight (the maximum weight value is one) to realise the control of the upper limit of the weight (Figure 1). In this study, 30 data samples were analysed with each sample having 32 landmarks. There were three to six landmarks, where the D value was <1 mm, accounting for approximately 15%. In the SP function, there is no difference in the weights of high weight landmarks, and the weighting strategy of medium and low weight landmarks conforms to the characteristics of the power function. Therefore, the difference between high and low weights can be limited to a reasonable range to achieve weight optimisation.

Secondly, the OP function can effectively reduce the gradient difference of the weighting function through the horizontal translation of the original power function. This narrows the scope of the value domain and also limits the maximum weight to one.

Meanwhile, the weight factor difference between different landmarks is reduced accordingly. The expression of the two weighting functions effectively limits the high output value of the original power function W_i to ensure the monotonous decreasing function of the weight allocation of the landmark. Therefore, the optimal value domain ($0 \leq W \leq 1$) and overlap of the original and mirror landmark sets, which are more aligned with the experience of oral clinical experts, is realised.

The results showed that the SRPs of the PWPA algorithm were closer to the truth plane (Figure 3). The SRP of an algorithm based on professional expertise was regarded as the truth plane in this study, which led to no significant difference from that constructed by experienced clinicians' visual determination (De Momi et al., 2006). The average angle error of the PWPA groups for the 30 patients with mandibular deviation was $<2^\circ$, and there was no significant difference between the SPWPA algorithm and the OPWPA algorithm. Wu et al. (2016) showed that the angle difference between the two planes is easily perceived when it is $>6^\circ$. In this study, the angle error between the PWPA SRP and the truth plane was $<2^\circ$, indicating that the accuracy of the PWPA SRP was almost equal to that of the truth plane; the result was lower than that compared with the angle error of 1.66° in our previous study (Zhu et al., 2020). Therefore, PWPA had better clinical suitability than the PA traditional algorithm.

Although establishing the SRP is the first fundamental step in the accurate analysis of facial asymmetry and craniomaxillofacial surgery planning, few studies have assessed the methods of establishing the SRP, such as the indices of angle error and facial asymmetry, which are mainly used to evaluate the accuracy of the SRP of the skull or face (Tan et al., 2019; Willing et al., 2013). The present study used position error as an SRP evaluation index 'position error'

to quantitatively analyse facial landmark asymmetry. It was designed to determine the weight of the PWPA algorithm landmarks and professional landmarks (implied empirical information) by calculating the distance between corresponding landmarks. The position error is small if the two weights are coincident and the mirror landmark overlap is apposite. The mirror landmarks differed between the experimental groups in mirroring the original facial model, whereas the original model was the same between the experimental and truth groups.

The finding of the position error reflects the coherence between the SRP of the PWPA algorithm and expert experience, realising the weight allocation of the overall facial landmarks. The mean values of the overall position errors of the PWPA and PA algorithms were 2.99, 2.98, and 4.08 mm, and there were statistical differences between the PWPA and PA algorithms (Table 1). This result shows that the overall superposing degree of mirrored features and weight allocation between the PWPA algorithm and professional experience was more precise than that between the PA algorithm and professional experience, the result in this study was lower than that in our previous study (3.64 mm) (Zhu et al., 2020); thus, the weight factor of the PWPA algorithm had a significant effect. The mean value of the regional position error (upper, middle and lower partitions) of the landmarks also showed that the SRP of the PWPA algorithm is more consistent with expert experience in the weight allocation of landmarks for each facial partition. The landmarks in the lower third of the face have a higher prevalence of asymmetry than those in the middle and upper thirds, where the deviation of the pogonion has been a point of particular interest (Kim et al., 2015). For patients with facial asymmetry in the mandibular region, landmarks in the lower part of the face are higher than those in the middle and upper parts. Consequently, the weight allocation of features in different regions is expected to vary and cannot be analysed using the overall position error. Therefore, the regional position error of the three facial regions was also calculated. For all three face partitions, the average position error of the PWPA algorithm was smaller than that of the PA algorithm. This difference was statistically significant, indicating that the PWPA algorithm for each facial partition was close to the result of professional judgement. Additionally, the position error of the PWPA algorithm for the upper and lower parts of the face was considerably smaller than that of the PA algorithm; this is because the PWPA algorithm allocated a lower weight for lower facial landmarks to reduce their influence on the global overlapping degree, whereas the upper landmarks were assigned higher weights to increase the overlapping degree, thereby accounting for professional experience in the weight allocation of the landmarks. The position error of the PWPA in each region was optimised compared with that of the PA algorithm without weight allocation, and an optimal SRP result was obtained.

There are several limitations to this study. Firstly, instead of selecting landmarks manually, automated identification of facial anatomical landmarks through artificial intelligence or a mathematical facial mask could effectively improve the automation of the

algorithm (Claes, Walters, & Clement, 2012; Claes, Walters, Shriver, et al., 2012; Claes et al., 2011; Gao et al., 2017; Lu et al., 2017; Walters et al., 2013; Zeng et al., 2018). This was a methodological study where we quantitatively analysed cases of mandibular deviation of <16 mm, and more sample cases are needed to analyse the applicability of our method for different types and degrees of facial deformities to provide guidance for clinical application. Secondly, the weight factors of the landmarks were indirectly acquired. The global ICP algorithm was used to initialise the superimposition of the original and mirror models to set the key parameters. Direct morphological feature analysis and deep-learning technology are potential means to solve this limitation, which can further improve the accuracy and rationality of landmark weight allocation and lead to better SRP constructions for simulating expert clinical diagnosis. Despite these limitations, we were able to draw some interesting conclusions related to the novel mathematical algorithm. The method is restricted neither to facial images nor to skeletal models. It can be applied to any surface model and in any anatomical area of the body. For example, it could be used with a model of the facial skeleton obtained from CBCT to assist during reconstruction planning with accurate mirrored templates. Two functions of the mathematical algorithm allow SRP computation for different degrees of facial asymmetry, according to each individual case and need.

5 | CONCLUSIONS

In this paper, we presented a novel mathematical algorithm to construct 3D facial SRPs for patients with mandibular deviation. The PWPA SRP was more closely aligned with the ground truth than the traditional PA SRP plane in terms of angle error and overall and regional position errors, indicating that our innovative mathematical algorithm accurately constructed SRPs for facial asymmetry in patients with mandibular deviation. In addition, the new mathematical method is not restricted to 3D facial data; it can also be applied to skeletal models. In a follow-up study, we will provide a new approach for dental clinics.

ACKNOWLEDGEMENTS

We thank the Peking University School and Hospital of Stomatology for assisting in the collection of clinical patient data. We further thank Dr Jie Liang, Dr Hu Chen and Dr Hongqiang Ye for their efforts in placing landmarks and selecting facial symmetry regions on the original models.

CONFLICT OF INTEREST

The authors declare that they have no competing interests.

AUTHOR CONTRIBUTIONS

Y. Zhu contributed to data acquisition, statistical analysis, data interpretation and drafted the manuscript. Y. Wang contributed to the conception, design and data acquisition and interpretation. X. Fu contributed to design, algorithm programming and revised the

manuscript. Lei Zhang contributed to the conception and revised the manuscript. S. Zheng contributed to the design and developed algorithm programming in Python. A. Wen and N. Xiao contributed to data acquisition and statistical analysis. Y. Zhao contributed to the conception, design and critically revised the manuscript. All authors gave their final approval and agree to be accountable for all aspects of the work.

ETHICS APPROVAL AND CONSENT TO PARTICIPATE

This study was approved by the Biomedical Ethics Committee of Peking University School and Hospital of Stomatology (No: PKUSSIRB-202054042). We declare that written informed consent was obtained from all participants included in the study.

CONSENT FOR PUBLICATION

Written informed consent to publish individual person's images was obtained.

DATA AVAILABILITY STATEMENT

The datasets used and analysed during the current study are available from the corresponding author on reasonable request.

ORCID

Yujia Zhu  <https://orcid.org/0000-0001-9234-5783>

REFERENCES

- Ai-Rudainy, D., Ju, X., Mehendale, F. & Ayoub, A. (2018) Assessment of facial asymmetry before and after the surgical repair of cleft lip in unilateral cleft lip and palate cases. *International Journal of Oral and Maxillofacial Surgery*, 47, 411–419.
- Al-Rudainy, D., Ju, X., Mehendale, F. & Ayoub, A. (2019a) The effect of facial expression on facial symmetry in surgically managed unilateral cleft lip and palate patients (UCLP). *Journal of Plastic Reconstructive and Aesthetic Surgery*, 72, 273–280.
- Al-Rudainy, D., Ju, X., Mehendale, F.V. & Ayoub, A. (2019b) Longitudinal 3D assessment of facial asymmetry in unilateral cleft lip and palate. *Cleft Palate-Craniofacial Journal*, 56, 495–501.
- Berssenbrügge, P., Lingemann-Koch, M., Abeler, A., Runte, C., Jung, S., Kleinheinz, J. et al. (2015) Measuring facial symmetry: a perception-based approach using 3D shape and color. *Biomedizinische Technik Biomedical Engineering*, 60, 39–47.
- Besl, P. & McKay, N. (1992) Method for registration of 3-D shapes. *IEEE Transactions on Pattern Analysis & Machine Intelligence*, 14, 239–256.
- Chen, Y. & Medioni, G. (1992) Object modeling by registration of multiple range images. *Image and Vision Computing*, 10, 145–155.
- Claes, P., Walters, M. & Clement, J. (2012) Improved facial outcome assessment using a 3D anthropometric mask. *International Journal of Oral and Maxillofacial Surgery*, 41, 324–330.
- Claes, P., Walters, M., Shriver, M.D., Puts, D., Gibson, G., Clement, J. et al. (2012) Sexual dimorphism in multiple aspects of 3D facial symmetry and asymmetry defined by spatially dense geometric morphometrics. *Journal of Anatomy*, 221, 97–114.
- Claes, P., Walters, M., Vandermeulen, D. & Clement, J.G. (2011) Spatially-dense 3D facial asymmetry assessment in both typical and disordered growth. *Journal of Anatomy*, 219, 444–455.
- Damstra, J., Fourie, Z., Wit, M.D. & Ren, Y. (2011) A three-dimensional comparison of a morphometric and conventional cephalometric midsagittal planes for craniofacial asymmetry. *Clinical Oral Investigations*, 16, 285–294.
- De Momi, E., Chapuis, J., Pappas, I., Ferrigno, G., Hallermann, W., Schramm, A. et al. (2006) Automatic extraction of the mid-facial plane for cranio-maxillofacial surgery planning. *International Journal of Oral and Maxillofacial Surgery*, 35, 636–642.
- Djordjevic, J., Toma, A.M., Zhurov, A.I. & Richmond, S. (2014) Three-dimensional quantification of facial symmetry in adolescents using laser surface scanning. *European Journal of Orthodontics*, 36, 125–132.
- Du, S., Xu, Y., Wan, T., Hu, H., Zhang, S., Xu, G. et al. (2017) Robust iterative closest point algorithm based on global reference point for rotation invariant registration. *PLoS One*, 12, e0188039.
- Gao, Y., Ma, J. & Yuille, A.L. (2017) Semi-supervised sparse representation based classification for face recognition with insufficient labeled samples. *IEEE Transactions on Image Processing*, 26, 2545–2560.
- Gateno, J., Jajoo, A., Nicol, M. & Xia, J.J. (2015) The primal sagittal plane of the head: a new concept. *International Journal of Oral & Maxillofacial Surgery*, 45, 399–405.
- Grammer, K. & Thornhill, R. (1994) Human (*Homo sapiens*) facial attractiveness and sexual selection: the role of symmetry and averageness. *Journal of Comparative Psychology*, 108, 233–242.
- Haraguchi, S., Iguchi, Y. & Takada, K. (2008) Asymmetry of the face in orthodontic patients. *Angle Orthodontist*, 78, 421–426.
- Hartmann, J., Meyer-Marcotty, P., Benz, M., Haeusler, G. & Stellzig-Eisenhauer, A. (2007) Reliability of a method for computing facial symmetry plane and degree of asymmetry based on 3D-data. *Journal of Orofacial Orthopedics-Fortschritte Der Kieferorthopädie*, 68, 477–490.
- Hönn, M., Dietz, K., Godt, A. & Göz, G. (2005) Perceived relative attractiveness of facial profiles with varying degrees of skeletal anomalies. *Journal of Orofacial Orthopedics*, 66, 187–196.
- Hönn, M. & Göz, G. (2007) The ideal of facial beauty: a review. *Journal of Orofacial Orthopedics*, 68, 6–16.
- Huang, C.S., Liu, X.Q. & Chen, Y.R. (2013) Facial asymmetry index in normal young adults. *Orthodontics & Craniofacial Research*, 16, 97–104.
- Hyeon-Shik, H., Yuan, D., Kweon-Heui, J., Gi-Soo, U., Jin-Hyoung, C. & Sook-Ja, Y. (2012) Three-dimensional soft tissue analysis for the evaluation of facial asymmetry in normal occlusion individuals. *Korean Journal of Orthodontics*, 42, 56–63.
- Kim, M.S., Lee, E.J., Song, I.J., Lee, J.-S., Kang, B.-C. & Yoon, S.-J. (2015) The location of midfacial landmarks according to the method of establishing the midsagittal reference plane in three-dimensional computed tomography analysis of facial asymmetry. *Imaging Science in Dentistry*, 45, 227–232.
- Lee, J.K., Jung, P.K. & Moon, C.H. (2014) Three-dimensional cone beam computed tomographic image reorientation using soft tissues as reference for facial asymmetry diagnosis. *Angle Orthodontist*, 84, 38–47.
- Lee, M.-S., Chung, D.H., Lee, J.-W. & Cha, K.-S. (2010) Assessing soft-tissue characteristics of facial asymmetry with photographs. *American Journal of Orthodontics and Dentofacial Orthopedics*, 138, 23–31.
- Linde, V.D. & Houle, D. (2009) Inferring the nature of allometry from geometric data. *Evolutionary Biology*, 36, 311–322.
- Lu, J., Wang, G. & Zhou, J. (2017) Simultaneous feature and dictionary learning for image set based face recognition. *IEEE Transactions on Image Processing*, 26, 4042–4054.
- Masoud, M.I., Bansal, N., C. Castillo, J., Manosudprasit, A., Allareddy, V., Haghi, A. et al. (2016) 3D dentofacial photogrammetry reference values: a novel approach to orthodontic diagnosis. *European Journal of Orthodontics*, 39, 215–225.
- Mealey, L., Bridgstock, R. & Townsend, G.C. (1999) Symmetry and perceived facial attractiveness: a monozygotic co-twin comparison. *Journal of Personality and Social Psychology*, 76, 151–158.
- Murakami, D., Inada, E., Saitoh, I., Takemoto, Y., Morizono, K., Kubota, N. et al. (2014) Morphological differences of facial soft tissue contours

- from child to adult of Japanese males: a three-dimensional cross-sectional study. *Archives of Oral Biology*, 59, 1391–1399.
- O'Grady, K.F. & Antonyshyn, O.M. (1999) Facial asymmetry: three-dimensional analysis using laser surface scanning. *Plastic and Reconstructive Surgery*, 104, 928–937.
- Philipp, M.M., Angelika, S.E., Ute, B., Jutta, H. & Janka, K. (2011) Three-dimensional perception of facial asymmetry. *European Journal of Orthodontics*, 33, 647–653.
- Plooij, J.M., Swennen, G., Rangel, F.A., Maal, T., Schutyser, F., Bronkhorst, E.M. et al. (2009) Evaluation of reproducibility and reliability of 3D soft tissue analysis using 3D stereophotogrammetry. *International Journal of Oral and Maxillofacial Surgery*, 38, 267–273.
- Shaner, D.J., Peterson, A.E., Beattie, O.B. & Bamforth, J.S. (2000) Assessment of soft tissue facial asymmetry in medically normal and syndrome-affected individuals by analysis of landmarks and measurements. *American Journal of Medical Genetics*, 93, 143–154.
- Stewart, C.V., Tsai, C.L. & Roysam, B. (2003) The dual-bootstrap iterative closest point algorithm with application to retinal image registration. *IEEE Transactions on Medical Imaging*, 22, 1379–1394.
- Tan, W., Kang, Y., Dong, Z., Chen, C., Yin, X., Su, Y. et al. (2019) An approach to extraction midsagittal plane of skull from brain CT images for oral and maxillofacial surgery. *IEEE Access*, 7, 203–217.
- Torcida, S., Gonzalez, P. & Lotto, F. (2016) A resistant method for landmark-based analysis of individual asymmetry in two dimensions. *Quantitative Biology*, 4, 270–282.
- Verhoeven, T.J., Coppen, C., Barkhuysen, R., Bronkhorst, E.M., Merx, M., Bergé, S.J. et al. (2013a) Three dimensional evaluation of facial asymmetry after mandibular reconstruction: validation of a new method using stereophotogrammetry. *International Journal of Oral and Maxillofacial Surgery*, 42, 19–25.
- Verhoeven, T.J., Nolte, J.W., Maal, T.J.J., Berge, S.J. & Becking, A.G. (2013b) Unilateral condylar hyperplasia: a 3-dimensional quantification of asymmetry. *PLoS One*, 8, e59391.
- Verhoeven, T., Xi, T., Schreurs, R., Bergé, S. & Maal, T. (2016) Quantification of facial asymmetry: a comparative study of landmark-based and surface-based registrations. *Journal of Cranio Maxillofacial Surgery*, 44, 1131–1136.
- Walters, M., Claes, P., Kakulas, E. & Clement, J.G. (2013) Robust and regional 3D facial asymmetry assessment in hemimandibular hyperplasia and hemimandibular elongation anomalies. *International Journal of Oral and Maxillofacial Surgery*, 42, 36–42.
- Willing, R.T., Roumeliotis, G., Jenkyn, T.R. & Yazdani, A. (2013) Development and evaluation of a semi-automatic technique for determining the bilateral symmetry plane of the facial skeleton. *Medical Engineering & Physics*, 35, 1843–1849.
- Wu, J., Heike, C., Birgfeld, C., Evans, K., Maga, M., Morrison, C. et al. (2016) Measuring symmetry in children with unrepaired cleft lip: defining a standard for the three-dimensional mid-facial reference plane. *Cleft Palate-Craniofacial Journal*, 53, 695–704.
- Xiong, Y., Zhao, Y., Yang, H., Sun, Y. & Wang, Y. (2016) Comparison between interactive closest point and Procrustes analysis for determining the median sagittal plane of three-dimensional facial data. *Journal of Craniofacial Surgery*, 27, 441–444.
- Zaidel, D.W., Aarde, S.M. & Baig, K. (2005) Appearance of symmetry, beauty, and health in human faces. *Brain and Cognition*, 57, 261–263.
- Zaidel, D.W. & Cohen, J.A. (2005) The face, beauty, and symmetry: perceiving asymmetry in beautiful faces. *International Journal of Neuroscience*, 115, 1165–1173.
- Zeng, J., Liu, S., Li, X., Mahdi, D.A., Wu, F. & Wang, G. (2018) Deep context-sensitive facial landmark detection with tree-structured modeling. *IEEE Transactions on Image Processing*, 27, 2096–2107.
- Zhu, Y., Zheng, S., Yang, G., Fu, X., Xiao, N., Wen, A. et al. (2020) A novel method for 3D face symmetry reference plane based on weighted Procrustes analysis algorithm. *BMC Oral Health*, 20.

How to cite this article: Zhu, Y., Fu, X., Zhang, L., Zheng, S., Wen, A., Xiao, N., et al (2021) A mathematical algorithm of the facial symmetry plane: Application to mandibular deformity 3D facial data. *Journal of Anatomy*, 00, 1–11. <https://doi.org/10.1111/joa.13564>